JOURNAL OF COMPUTATIONAL PHYSICS 79, 113–134 (1988)

Unsteady Solution of Incompressible Navier–Stokes Equations

W. Y. SOH

Sverdrup Technology Inc., and NASA Lewis Research Center, Cleveland, Ohio 44135

AND

JOHN W. GOODRICH

Computational Fluid Dynamics Branch, NASA Lewis Research Center, Cleveland, Ohio 44135

Received April 30, 1987; revised January 22, 1988

A new time-accurate finite-difference numerical method for solving incompressible Navier–Stokes equations is presented with primitive variables as the unknowns. The numerical scheme is a Crank–Nicolson implicit treatment of all terms of the equations with central differencing for space derivatives. The pressure and the nonlinearities in convection terms are not lagged. To obtain the incompressible solution at the advanced time level a continuous auxiliary system is introduced in pseudo time with artificial compressibility. Time-accurate solutions are presented for two-dimensional fluid flows in a square cavity with an impulsively starting lid and with an oscillating lid.

1. INTRODUCTION

Solution of the incompressible Navier–Stokes equations is of great interest in fluid mechanics since the fluid motion of water and low speed air is considered incompressible. There are also many other engineering applications. This paper is concerned with unsteady solutions of fluid motion whether they approach an ultimate steady state or not.

A significant difficulty for incompressible flow calculations occurs since the continuity equation is given not in a time evolution form, but in the form of a divergence-free constraint. This is one of the major differences from compressible flow calculations. The pressure, which has no time term, is coupled implicitly with the divergence-free constraint on the velocity. This constraint, which is the continuity equation, prohibits time integration of the incompressible flow equations in a straightforward manner.

Due to the special role of the pressure, approaches to the solution of the Navier–Stokes equations may be classified into three major areas. The first

0021-9991/88 $3.00

approach solves for vorticity as a primary unknown from the vorticity transport equation which is constructed by taking the curl of the momentum equation. The continuity constraint is satisfied by introduction of the vector potential for velocity. For two-dimensional flow the vector potential has only one component, which is the streamfunction. This vorticity-streamfunction method (see Ref. [1]) has been widely used for calculating fluid flow in two space dimensions.

The second approach is a fractional step method with a primitive variable formulation, in which an intermediate step is introduced to yield a velocity field satisfying only the momentum equation with no pressure term. To obtain a velocity of zero divergence, the intermediate velocity and the pressure are corrected sequentially by the pressure gradient, and by the divergence of the intermediate velocity, respectively. This approach, which is now known as the projection method, has been developed by Chorin [2]. Recent work with this idea has been done by Kim and Moin [3]. A variant form of [2] called the velocity-pressure method [4] also calculates the intermediate velocity from the momentum equation but with the pressure term. The pressure is then corrected by an amount proportional to the divergence of velocity and a new velocity is obtained successively until the divergence of velocity vanishes. Peyret [5] follows this iterative procedure to obtain the solution of nonlinear system of equations via the Crank–Nicolson approximation of all terms.

The third method may be viewed as a coupling between the momentum and the continuity equations. This method can be subdivided into two types; indirect and direct coupling. The former calls for the solution of a Poisson equation for the pressure, which is derived by taking the divergence of the momentum equation combined with continuity. This approach, known as the pressure Poisson method, has been introduced by Harlow and Welch [6] for the solution of two-dimensional flow and extended to three dimensions by Williams [7]. Moin and Kim [8] have used the latter approach which solves the momentum and continuity equations simultaneously to yield the velocity and pressure. The former method is here referred to as the indirect coupling because of the sequential treatment of the momentum and Poisson equations to yield the pressure and divergence-free velocity.

In this paper we present a new time accurate finite-difference method for incompressible fluid flow, which is different from any of the three approaches discussed above. The Crank–Nicolson approximation is used for all linear and nonlinear terms, including pressure. A pseudo-time is introduced between the two physical time steps in order to solve the nonlinear system for the divergence-free velocity at the advanced time level. The momentum equations are discretized in physical time and are then written in a continuous pseudo-time derivative form. The continuity equation is preconditioned with a pseudo-time derivative of the pressure. The artificial compressibility method [9] is applied to the preconditioned system of equations in the pseudo-time domain. This method provides an enormous computational economy in a steady-state incompressible flow calculation because it does not require a divergence-free velocity field at every time step until the steady

state is reached. The physical solution at the advanced time level is obtained as the steady solution of the system of preconditioned equations in the pseudo-time.

Most previous methods generally avoid solving nonlinear equations by an explicit treatment of the convection terms, for example, by simply lagging these terms or by using the second-order Adams–Bashforth method. This imposes a severe constraint on the time step size in terms of the Courant number limit. In the present work the Courant number limit on the physical time step is eliminated by the use of the Crank–Nicolson approximation for all terms and by coupling the momentum equations with the continuity in an appropriate manner. The mathematical formulation is described in Section 2. Computational results are presented in Section 3 for fluid flows in a driven cavity. As example problems, two-dimensional unsteady solutions are presented for fluid flows in a square cavity with an impulsively starting lid and with an oscillating lid.

2. FORMULATION

The incompressible Navier–Stokes equations are written in a dimensionless form as

$$\frac{\partial \mathbf{u}}{\partial t} + \nabla \cdot (\mathbf{uu}) + \nabla p - \frac{1}{\mathrm{Re}} \nabla^2 \mathbf{u} = 0 \tag{1}$$

and

$$\nabla \cdot \mathbf{u} = 0, \tag{2}$$

where $\mathbf{u}$ is the velocity, p the static pressure, t the time, and Re the Reynolds number. It is our aim to solve (1) accurately in time and space with the constraint (2). Using the standard Crank–Nicolson approximation for discretizing the momentum equation (1) with respect to time gives

$$\frac{\mathbf{u}^{n+1} - \mathbf{u}^n}{\Delta t} + \frac{1}{2}[\mathbf{G}(\mathbf{u}^{n+1}, p^{n+1}) + \mathbf{G}(\mathbf{u}^n, p^n)] = 0, \tag{3}$$

where Δt is the time increment, the superscripts n and $n+1$ refer to the time levels, and $\mathbf{G}(\mathbf{u}, p) = \nabla \cdot (\mathbf{uu}) + \nabla p - \mathrm{Re}^{-1} \nabla^2 \mathbf{u}$. The time difference equation (3) has second-order accuracy in time, but it is nonlinear since the convection terms are also evaluated at the $n+1$ time step. The continuity equation (2) should be satisfied at every time step, so

$$\nabla \cdot \mathbf{u}^{n+1} = 0. \tag{4}$$

If we write $\hat{\mathbf{u}}^{n+1} = \mathbf{u}^{n+1} - \mathbf{u}^n$ and $\hat{p}^{n+1} = p^{n+1} - p^n$, then Eqs. (3) and (4) are rewritten as

$$\hat{\mathbf{u}}^{n+1} + \alpha \mathbf{G}(\mathbf{u}^n + \hat{\mathbf{u}}^{n+1}, p^n + \hat{p}^{n+1}) = -\alpha \mathbf{G}(\mathbf{u}^n, p^n) \tag{5}$$

$$\nabla \cdot \hat{\mathbf{u}}^{n+1} = 0, \tag{6}$$

where $\alpha = \Delta t/2$. For the nonlinear solution of (5) satisfying the divergence-free constraint (6) on the velocity, we introduce a continuous auxiliary system in pseudo-time, as

$$\frac{\partial \hat{\mathbf{u}}}{\partial \tau} + \hat{\mathbf{u}} + \alpha \mathbf{G}(\mathbf{u}^n + \hat{\mathbf{u}}, p^n + \hat{p}) = -\alpha \mathbf{G}(\mathbf{u}^n, p^n) \tag{5'}$$

$$\beta \frac{\partial \hat{p}}{\partial \tau} + \nabla \cdot \hat{\mathbf{u}} = 0 \tag{6'}$$

where τ is the *pseudo-time* which is not physical, β is the artificial compressibility coefficient, and $\hat{\mathbf{u}} = \mathbf{u}^* - \mathbf{u}^n$, $\hat{p} = p^* - p^n$; here, the asterisk denotes a transient value in pseudo-time. From (5′) and (6′) we can see that $\hat{\mathbf{u}}$ and $\hat{p}$ become $\hat{\mathbf{u}}^{n+1}$ and $\hat{p}^{n+1}$, respectively, as the steady state is reached asymptotically in pseudo-time. Consequently, the solution of the system (5) and (6) is equivalent to the steady solution of the system (5′) and (6′). The time τ is called here *pseudo-time* to be distinguished from the *physical time t*. As we see in (6′), the divergence-free velocity field is not obtained until the steady state is reached. Therefore, the system (5′) and (6′) has no physical meaning until reaching the steady state in pseudo-time. Since the pseudo-time τ is purely artificial the time increment $\Delta\tau$ can be taken as large as possible to expedite the convergence to the steady state. This artificial compressibility method has been used for the steady solution of various fluid flow problems [9–12].

Dropping the superscript n for convenience and writing the components of (5′) and (6′) in the Cartesian coordinates (x, y) gives

$$\frac{\partial \hat{u}}{\partial \tau} + \hat{u} + \alpha \left[\frac{\partial}{\partial x}(2u\hat{u} + \hat{u}^2 + \hat{p}) + \frac{\partial}{\partial y}(u\hat{v} + v\hat{u} + \hat{u}\hat{v}) - \mathrm{Re}^{-1} \nabla^2 \hat{u} \right] = -2\alpha G_x \tag{7}$$

$$\frac{\partial \hat{v}}{\partial \tau} + \hat{v} + \alpha \left[\frac{\partial}{\partial x}(u\hat{v} + v\hat{u} + \hat{u}\hat{v}) + \frac{\partial}{\partial y}(2v\hat{v} + \hat{v}^2 + \hat{p}) - \mathrm{Re}^{-1} \nabla^2 \hat{v} \right] = -2\alpha G_y \tag{8}$$

$$\beta \frac{\partial \hat{p}}{\partial \tau} + \frac{\partial \hat{u}}{\partial x} + \frac{\partial \hat{v}}{\partial y} = 0, \tag{9}$$

where $(\hat{u}, \hat{v})$ and (u, v) are the Cartesian components of the velocities, and where G_x and G_y in (7) and (8) are the Cartesian components of $\mathbf{G}(\mathbf{u}, p)$,

$$G_x = \frac{\partial u^2}{\partial x} + \frac{\partial}{\partial y}(uv) + \frac{\partial p}{\partial x} - \mathrm{Re}^{-1} \nabla^2 u$$

$$G_y = \frac{\partial}{\partial x}(uv) + \frac{\partial v^2}{\partial y} + \frac{\partial p}{\partial y} - \mathrm{Re}^{-1} \nabla^2 v.$$

The values of (u, v) in (7) and (8) appearing as coefficients of $(\hat{u}, \hat{v})$ are the values at the physical time step n. The terms $(-2\alpha G_x, -2\alpha G_y)$ in (7) and (8) are evaluated at the physical time step n, and they serve as external forcing terms that drive the flow variables from the physical time step n to $n+1$. The system (7), (8), and (9) may be considered as a continuous version of a Newton type iterative method for solving the nonlinear equations (3) and (4). If we let $u^{n,k}$, $v^{n,k}$, and $p^{n,k}$ be the kth estimates of u^{n+1}, v^{n+1}, and p^{n+1} in Newton's method for (3) and (4), with u^n, v^n, and p^n as our initial guess, then the component equations for $\Delta u = u^{n,k+1} - u^{n,k}$, $\Delta v = v^{n,k+1} - v^{n,k}$, and $\Delta p = p^{n,k+1} - p^{n,k}$ are

$$\begin{aligned}
&\Delta u + \alpha\left[\frac{\partial}{\partial x}(2u\Delta u + \Delta p) + \frac{\partial}{\partial y}(u\Delta v + v\Delta u) - \mathrm{Re}^{-1}\nabla^2(\Delta u)\right] \\
&\quad = -u^{n,k} + u^n - \alpha(G_x^n + G_x^{n,k}) \\
&\Delta v + \alpha\left[\frac{\partial}{\partial x}(u\Delta v + v\Delta u) + \frac{\partial}{\partial y}(2v\Delta v + \Delta p) - \mathrm{Re}^{-1}\nabla^2(\Delta v)\right] \\
&\quad = -v^{n,k} + v^n - \alpha(G_y^n + G_y^{n,k}) \qquad (10) \\
&\frac{\partial}{\partial x}(\Delta u) + \frac{\partial}{\partial y}(\Delta v) = 0.
\end{aligned}$$

In the previous section, the direct solution of (10) is referred to as the direct coupling approach. The system used by Moin and Kim [8] is the same as this, except that theirs is linear due to an explicit treatment of the convection terms and no iterative procedure is needed (i.e., $k=0$) for the solution of the coupled system (10).

Since the physical time system (3) and (4) or (5) and (6), and the pseudo-time system (5′) and (6′), are both initial boundary value problems, initial and boundary data must be specified to complete these systems. Any divergence-free velocity field, with arbitrary pressure distribution may be admitted as initial data for system (3) and (4), and the initial flow variables for system (5′) and (6′) are taken to be zero:

$$\text{any } \mathbf{u} \text{ and } p \text{ satisfying } \nabla\cdot\mathbf{u} = 0 \qquad \text{at} \quad t = 0$$

and

$$\hat{\mathbf{u}} = \hat{p} = 0 \qquad \text{at} \quad \tau = 0. \qquad (11)$$

For boundary conditions, let us consider the case of a driven cavity flow where the velocity is given along boundaries (boundary conditions for a through flow problem are different and will not be considered here). We will employ the staggered mesh shown in Fig. 1, so that the boundaries on which the velocity is given are half a mesh space from any pressure locations, and pressure boundary

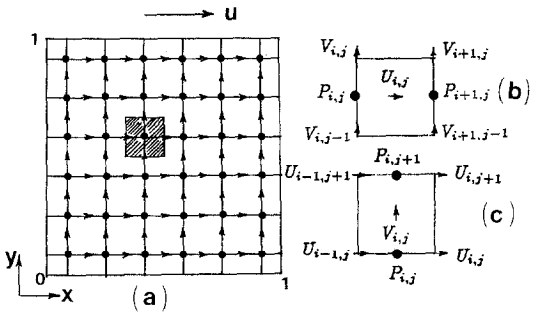

FIG. 1. (a) Schematic of staggered grids for a cavity geometry: ●, pressure; →, u-; ↑, v-velocity. Shaded area represents p-cell. (b) u-cell. (c) v-cell.

conditions are not needed. The velocity boundary conditions for the two systems are

$$\begin{aligned} &u = v = \hat{u} = \hat{v} = 0 \qquad \text{at} \quad x = 0, x = 1, y = 0. \\ &u = U_B(t) \qquad \text{and} \qquad \hat{u} = U_B(t^{n+1}) - U_B(t^n) \qquad \text{at} \quad y = 1. \end{aligned} \tag{12}$$

where $U_B(t)$ is the velocity of the lid. The boundary value of $\hat{u}$ at $y = 1$ is taken as if the steady state were reached because in system (5′) and (6′) transient values of $\hat{u}$ at $y = 1$ cannot be clearly defined. However, this boundary value of $\hat{u}$ at $y = 1$ becomes exact as the solution approaches steady state in pseudo-time.

Various explicit or implicit numerical schemes may be used for the solution of Eqs. (7)–(9) in pseudo-time. In the present study we employ a factored alternating direction implicit scheme. If the superscript k denotes the pseudo-time level, then the y-sweep from (8) and (9) for our scheme may be written as

$$\begin{aligned} &\frac{\hat{v}^{k+1} - \hat{v}^k}{\Delta\tau} + \hat{v}^{k+1} + \alpha \frac{\partial}{\partial y}\left[2v\hat{v}^{k+1} + \bar{p}^{k+1} - \mathrm{Re}^{-1}\frac{\partial \hat{v}^{k+1}}{\partial y}\right] = H_y \\ &\beta \frac{\bar{p}^{k+1} - \hat{p}^k}{\Delta\tau} + \frac{\partial \hat{v}^{k+1}}{\partial y} = -\frac{\partial \hat{u}^k}{\partial x}, \end{aligned} \tag{13}$$

where $\bar{p}^{k+1}$ is an intermediate value of $\hat{p}^{k+1}$, and

$$H_y = -\alpha\left[2G_y + \frac{\partial}{\partial x}\left(u\hat{v}^k + v\hat{u}^k + \hat{u}^k\hat{v}^k - \mathrm{Re}^{-1}\frac{\partial \hat{u}^k}{\partial x}\right) + \frac{\partial}{\partial y}(\hat{v}^2)^k\right].$$

The *y-sweep* is followed by the *x-sweep* from (7) and (9), with

$$\begin{aligned} &\frac{\hat{u}^{k+1} - \hat{u}^k}{\Delta\tau} + \hat{u}^{k+1} + \alpha \frac{\partial}{\partial x}\left[2u\hat{u}^{k+1} + \hat{p}^{k+1} - \mathrm{Re}^{-1}\frac{\partial \hat{u}^{k+1}}{\partial x}\right] = H_x \\ &\beta \frac{\hat{p}^{k+1} - \hat{p}^k}{\Delta\tau} + \frac{\partial \hat{u}^{k+1}}{\partial x} = -\frac{\partial \hat{v}^{k+1}}{\partial y}, \end{aligned} \tag{14}$$

where

$$H_x = -\alpha\left[2G_x + \frac{\partial}{\partial y}\left(u\hat{v}^k + v\hat{u}^k + \hat{u}^k\hat{v}^k - \mathrm{Re}^{-1}\frac{\partial \hat{u}^k}{\partial y}\right) + \frac{\partial}{\partial x}(\hat{u}^2)^k\right].$$

In the y-sweep, $\hat{v}$ is coupled with the pressure and is considered to have only y derivatives, with all x derivatives and nonlinearities lagged and absorbed in H_y. In the x-sweep, $\hat{u}$ is coupled with the pressure and is assumed to have only x derivatives, with all y derivatives and nonlinearities absorbed in the source term H_x. Central difference approximations with a uniform staggered grid are used for the spatial discretization of (13) and (14). In this staggered grid finite-difference approximations of u, v, and p are made at different grid positions, called the u-, v-, and p-cells as shown in Fig. 1. Let the subscripts i and j be the indices in the x and y directions. Then, the central difference formulation of (13) in the y-sweep becomes

$$a_{j\ 1}\hat{v}_{ij-1}^{k+1} + a_j\hat{v}_{ij}^{k+1} + a_{j+1}\hat{v}_{ij+1}^{k+1} + \frac{\alpha\Delta\tau}{\Delta y}(\bar{p}_{ij+1}^{k+1} - \bar{p}_{ij}^{k+1}) = \hat{v}_{ij}^k - \Delta\tau H_y \tag{15}$$

$$\bar{p}_{ij}^{k+1} = \hat{p}_{ij}^k - \frac{\Delta\tau}{\beta\Delta y}(\hat{v}_{ij}^{k+1} - \hat{v}_{ij-1}^{k+1}) - \frac{\Delta\tau}{\beta\Delta x}(\hat{u}_{ij}^k - \hat{u}_{i+1j}^k), \tag{16}$$

where

$$a_{j-1} = -\alpha\Delta\tau\left(\frac{VVS}{\Delta y} + \frac{1}{\mathrm{Re}\,\Delta y^2}\right), \qquad a_j = 1 + \Delta\tau + \alpha\Delta\tau\left(\frac{VVN - VVS}{\Delta y} + \frac{2}{\mathrm{Re}\,\Delta y^2}\right),$$

$$a_{j+1} = \alpha\Delta\tau\left(\frac{VVN}{\Delta y} - \frac{1}{\mathrm{Re}\,\Delta y^2}\right),$$

and where VVS and VVN are the v-velocities on the north and sourth boundaries of the v-cell. The finite difference approximation of (14) in the x-sweep becomes

$$b_{i-1}\hat{u}_{i-1j}^{k+1} + b_i\hat{u}_{ij}^{k+1} + b_{i+1}\hat{u}_{i+1j}^{k+1} + \frac{\alpha\Delta\tau}{\Delta x}(\hat{p}_{i+1j}^{k+1} - \hat{p}_{ij}^{k+1}) = \hat{u}_{ij}^k - \Delta\tau H_x \tag{17}$$

$$\hat{p}_{ij}^{k+1} = \hat{p}_{ij}^k - \frac{\Delta\tau}{\beta\Delta x}(\hat{u}_{ij}^{k+1} - \hat{u}_{i-1j}^{k+1}) - \frac{\Delta\tau}{\beta\Delta y}(\hat{v}_{ij}^{k+1} - \hat{v}_{ij-1}^{k+1}), \tag{18}$$

where

$$b_{i-1} = -\alpha\Delta\tau\left(\frac{UUW}{\Delta x} + \frac{1}{\mathrm{Re}\,\Delta x^2}\right), \qquad b_i = 1 + \Delta\tau + \alpha\Delta\tau\left(\frac{UUE - UUW}{\Delta x} + \frac{2}{\mathrm{Re}\,\Delta x^2}\right),$$

$$b_{i+1} = \alpha\Delta\tau\left(\frac{UUE}{\Delta x} - \frac{1}{\mathrm{Re}\,\Delta x^2}\right),$$

and where UUE and UUW are the u-velocities on the east and west sides of the

u-cell. Details of the finite-difference expressions of H_x and H_y may be found in Ref. [12].

The system (15) and (16) yields a coupled solution of $\hat{v}^{k+1}$ and $\bar{p}^{k+1}$ through a 2×2 block tridiagonal coefficient matrix. If we obtain the term $\bar{p}_{ij+1}^{k+1}-\bar{p}_{ij}^{k+1}$ from (16) at mesh points (i,j) and $(i,j+1)$, and substitute the resulting expression into (15), we obtain the tridiagonal scalar equation

$$(a_{j-1}-e)\,\hat{v}_{ij-1}^{k+1}+(a_j+2e)\,\hat{v}_{ij}^{k+1}+(a_{j+1}-e)\,\hat{v}_{ij+1}^{k+1}$$
$$=\hat{v}_{ij}^{k}-\Delta\tau H_y-\frac{\alpha\Delta\tau}{\Delta y}\left[\frac{\Delta\tau}{\beta}\left(\frac{\partial\hat{u}_{ij}^{k}}{\partial x}-\frac{\partial\hat{u}_{ij+1}^{k}}{\partial x}\right)+\hat{p}_{ij+1}^{k}-\hat{p}_{ij}^{k}\right], \quad (15')$$

where

$$e=\alpha\Delta\tau^2/(\beta\Delta y^2), \qquad \partial\hat{u}_{ij}/\partial x=(\hat{u}_{ij}-\hat{u}_{i-1j})/\Delta x, \qquad \partial\hat{u}_{ij+1}/\partial x=(\hat{u}_{ij+1}-\hat{u}_{i-1j+1})/\Delta x.$$

In a similar manner, $\hat{u}^{k+1}$ is coupled with $\hat{p}^{k+1}$ in the x-sweep, so that (17) and (18) are combined to give the tridiagonal scalar equation

$$(b_{i-1}-f)\,\hat{u}_{i-1j}^{k+1}+(b_i+2f)\,\hat{u}_{ij}^{k+1}+(b_{i+1}-f)\,\hat{u}_{i+1j}^{k+1}$$
$$=\hat{u}_{ij}^{k}-\Delta\tau H_x-\frac{\alpha\Delta\tau}{\Delta x}\left[\frac{\Delta\tau}{\beta}\left(\frac{\partial\hat{v}_{ij}^{k+1}}{\partial y}-\frac{\partial\hat{v}_{i+1j}^{k+1}}{\partial y}\right)+\hat{p}_{i+1j}^{k}-\hat{p}_{ij}^{k}\right], \quad (17')$$

where

$$f=\alpha\Delta\tau^2/(\beta\Delta x^2), \qquad \partial\hat{v}_{ij}/\partial y=(\hat{v}_{ij}-\hat{v}_{ij-1})/\Delta y, \qquad \partial\hat{v}_{i+1j}/\partial y=(\hat{v}_{i+1j}-\hat{v}_{i+1j-1})/\Delta y.$$

The pressure p is then obtained by (18).

To see how to choose the coefficient of artificial compressibility β, we will consider the one-dimensional inviscid model problem from (5') and (6')

$$\frac{\partial}{\partial\tau}\begin{bmatrix}\hat{u}\\ \hat{p}\end{bmatrix}+\begin{bmatrix}2\alpha u & \alpha\\ 1/\beta & 0\end{bmatrix}\frac{\partial}{\partial x}\begin{bmatrix}\hat{u}\\ \hat{p}\end{bmatrix}=0. \quad (19)$$

In (19) nonderivative terms are also dropped for simplicity. The eigenvalues of the square matrix in (19) are

$$\lambda=\alpha u\pm(\alpha^2u^2+\alpha/\beta)^{1/2} \quad (20)$$

The eigenvalues (20) are real and distinct, so that the system (19) with artificial compressibility is hyperbolic in pseudo-time, and subsonic in the sense that the eigenvalues are opposite in sign. Since an eigenvalue of the system (19) is a wave propagation velocity, the λ's in (20) may be interpreted as waves travelling along and against the fluid flow with a sound-like velocity $(\alpha^2u^2+\alpha/\beta)^{1/2}$ relative to the local fluid flow. The local flow velocity in our system (19) is αu instead of u because that system was derived in the pseudo-time using the Crank–Nicolson time

discretization. For compressible flow with fluid velocity s and speed of sound c, the eigenvalues are s, $s+c$, and $s-c$, so that we may identify s and c with αu and $(\alpha^2 u^2 + \alpha/\beta)^{1/2}$ in the pseudo-time system. The choice of a value for β is optimal if the magnitude of the eigenvalues are close to each other, with

$$\alpha u \sim \alpha u + (\alpha^2 u^2 + \alpha/\beta)^{1/2} \sim (\alpha^2 u^2 + \alpha/\beta)^{1/2} - \alpha u.$$

A good compromise can be reached if we take β to be $1/(3\alpha u^2)$, so that the ratio of the largest to the smallest eigenvalues becomes only 3. In the present analysis we take β as

$$\beta = \frac{1}{\Delta t\, q^2}, \tag{21}$$

where q is a representative physical flow speed such as $(u^2+v^2)^{1/2}$. The choice of q is highly heuristic, especially for a fluid flow with no preferred flow direction. However, Eq. (21) provides a plausible guideline for choosing a value of β so that the product of the artificial compressibility and the kinetic energy is of order Δt^{-1}. The value of β can be taken much larger in the present unsteady calculation through the pseudo-time system than in the unsteady calculation for a steady solution, where βq^2 is of order unity.

We will examine the coupled systems (15′) and (17′) for velocity and pressure in order to choose a pseudo-time step $\Delta\tau$. If we assume that $VVN = VVS = v$ and $UUE = UUW = u$, with both positive, then diagonal dominance is kept in (15′) if $R_v < 1$ or $\Delta\tau \geqslant \beta v \Delta y(1 - R_v^{-1})$, or $\Delta\tau < \beta v \Delta y(1 - R_v^{-1})$ and $(v\Delta t/\Delta y)(1 - R_v^{-1}) > 1$, where R_v is the cell Reynolds number defined as $v\,\mathrm{Re}\,\Delta y$. Similarly, diagonal dominance is kept in (17′) if $R_u < 1$ or $\Delta\tau \geqslant \beta u \Delta x(1 - R_u^{-1})$, or $\Delta\tau < \beta u \Delta x(1 - R_u^{-1})$ and $(u\Delta t/\Delta x)(1 - R_u^{-1}) > 1$, where R_u is another cell Reynolds number $u\,\mathrm{Re}\,\Delta x$. The last condition for either (15′) or (17′) is interesting though impractical, since too small a value of $\Delta\tau$ requires the Courant numbers $\Delta t v/\Delta y$ and $\Delta t u/\Delta x$ to be larger than unity. In this paper we have neglected $1/R_v$ and $1/R_u$, and we have chosen the pseudo-time step as

$$\Delta\tau > \max(\beta \Delta y\, v_{\max},\ \beta \Delta x\, u_{\max}). \tag{22}$$

Condition (22) gives a lower limit on $\Delta\tau$ and numerical experiments are required to obtain an optimal value. The choice of the physical time step Δt depends upon the character of the problem under consideration. If the solution approaches a steady state, the Δt can be taken gradually larger as physical time goes on. If a problem has forced excitation, then Δt should be chosen to resolve the details of the excitation. For a study on flow behavior in large vortical structure such as in mixing layers of jets or coflows, Δt should be taken small in order to capture the vortex roll-up phenomena.

3. Numerical Results

Numerical results will now be presented for unsteady flows in a two-dimensional square cavity driven by the movement of the lid (i.e., $y = 1$). Flow in a driven cavity has drawn much attention because of its relevance to recirculating fluid flows in a confined area. It also has been chosen as a test problem for the numerical scheme developed since the boundary conditions are well defined, and since there is no preferred flow direction. Most effort has been spent on the steady solution of the two-dimensional flow using either a vorticity-streamfunction formulation [13, 14], or a primitive variable formulation [3, 12, 15].

Some unsteady solutions have recently been reported using vorticity and velocity as primary unknowns [16] and using primitive variables [17, 18, 19]. All of these results present the flow field with time after an impulsively started motion of the lid. In the present study we present unsteady solutions for a case in which the lid moves with a uniform velocity impulsively, and for a case where the lid oscillates periodically. The solution of the former case approaches steady state, but the latter case does not. A 40×40 uniform grid with $\Delta x = \Delta y = 0.025$ is used throughout, and the calculations are all at $\mathrm{Re} = 400$. The Reynolds number is defined as $\mathrm{Re} = U_0 L/\nu$, based upon the side length L, the kinematic viscosity ν, and the velocity U_0 taken as the uniform lid velocity for the case with an impulsively started lid, and as the maximum lid velocity for the case with an oscillating lid.

Flow Inside a Cavity with an Impulsively Started Lid

The velocity of the impulsively started lid is given by a step function $u_{lid} = U_0$ for $t \geqslant 0$ and $u_{\mathrm{lid}} = 0$ for $t < 0$. At the initial stage of flow development as $t \to 0^+$, a flow boundary layer forms along the lid away from the corners with the dimensionless thickness of $\delta \sim \sqrt{t/\mathrm{Re}}$. Since the boundary layer thickness is extremely small for $t \to 0^+$, it is very difficult to resolve this boundary layer numerically unless an enormous number of grid points are employed. If we estimate the boundary layer thickness to be 1/80, which is the grid generated boundary layer between the lid and the immediately neighboring location of u-velocity in the y-direction, then the time required for the growth of the boundary layer to this thickness is about 0.06 at $\mathrm{Re} = 400$. Under the grid arrangement used in this work the solution for $t \ll 0.06$ may not be appropriate for physical interpretation. For the flow with an impulsively started lid, a minimum time step of $\Delta t = 0.05$ is used at the beginning.

Since this example exhibits the typical behavior of an asymptotic approach to the steady state, the physical time step size, which is 0.05 initially, is increased up to 0.8 for large t. Table I lists with increasing t the coefficient of artificial compressibility, time step size, convergence criteria for reaching steady-state in the pseudo time, and others. Here, E_u and E_v denote the x and y components of $\partial \mathbf{u}/\partial t + \nabla \cdot (\mathbf{uu}) + \nabla p - 1/\mathrm{Re}\, \nabla^2 \mathbf{u}$, which are the u and v momentum equation residuals, and rms denotes the root-mean-square. The values with an asterisk in Table I are taken as the convergence criteria for reaching steady state in the pseudo-time. The velocity is very small in the entire cavity, except in a narrow region underneath the upper lid

TABLE I

	β	Δt	$\Delta\tau$	$\max(\nabla \cdot \mathbf{u})$	$\max(Eu)$	$\max(Ev)$	$\mathrm{rms}(Eu)$	$\mathrm{rms}(Ev)$	No. of $\Delta\tau$ steps
$0 < t \leqslant 2$	100	0.05	30	$* 1.0 \times 10^{-3}$	$8.3 \times 10^{-5} - 1.0 \times 10^{-4}$	$4.7 \times 10^{-4} - 2.6 \times 10^{-3}$	$1.5 \times 10^{-5} - 1.3 \times 10^{-5}$	$2.7 \times 10^{-5} - 1.1 \times 10^{-4}$	58 – 23
$2 < t \leqslant 4$	100	0.1	30	$2.7 \times 10^{-5} - 1.9 \times 10^{-5}$	$5.1 \times 10^{-5} - 4.4 \times 10^{-5}$	$* 2.0 \times 10^{-3}$	$2.0 \times 10^{-6} - 1.7 \times 10^{-6}$	$9.1 \times 10^{-5} - 7.9 \times 10^{-5}$	32
$4 < t \leqslant 8$	50	0.2	30	$8.4 \times 10^{-5} - 2.8 \times 10^{-4}$	$1.5 \times 10^{-4} - 5.1 \times 10^{-4}$	$* 3.0 \times 10^{-3}$	$1.7 \times 10^{-5} - 3.6 \times 10^{-5}$	$3.5 \times 10^{-4} - 3.1 \times 10^{-4}$	32 – 26
$8 < t \leqslant 20$	20	0.4	20	$1.2 \times 10^{-5} - 1.3 \times 10^{-5}$	$7.9 \times 10^{-5} - 9.8 \times 10^{-5}$	$* 3.0 \times 10^{-3}$	$7.9 \times 10^{-6} - 5.2 \times 10^{-6}$	$5.6 \times 10^{-4} - 2.7 \times 10^{-4}$	35 – 23
$20 < t \leqslant 36$	10	0.8	10	$3.9 \times 10^{-5} - 1.0 \times 10^{-4}$	$7.9 \times 10^{-5} - 1.9 \times 10^{-4}$	$* 3.0 \times 10^{-3}$	$8.6 \times 10^{-6} - 1.8 \times 10^{-5}$	$3.1 \times 10^{-4} - 3.0 \times 10^{-4}$	27 – 23

immediately after the impulsive motion, and the velocity increases as the flow evolves further. Consequently the value of β is taken as large as 100 in the beginning and then becomes reduced as suggested by (21).

The drag coefficient C_D is defined to be a dimensionless drag force exerted on the

$$C_D = \frac{\text{Drag force on the lid/length}}{\rho U_0^2 L} = \frac{D}{\text{Re}} \tag{23}$$

where

$$D = \int_0^1 \left(\frac{\partial u}{\partial y}\right)_{y=1} dx.$$

Three values of u are used to evaluate the wall shear $(\partial u/\partial y)_{y=1}$ in (23)

$$\left(\frac{\partial u}{\partial y}\right)_{y=1} \cong \frac{8u_{\text{lid}} - u_{iJ-1} + 9u_{iJ}}{3\Delta y}. \tag{24}$$

It is seen from Fig. 2 that immediately after the impulsive start of the lid, D decreases precipitously and then becomes quickly constant. Although the drag D exhibits a steady behavior in a very short time, it takes relatively long for the entire flow field to settle down to a steady state. To investigate the singular behavior of D as $t \to 0^+$ in Fig. 2, its values are plotted against $t^{-1/2}$ in Fig. 3. The D values 66.7, 48.9, 40.3, 35.8 corresponding in order to $t = 0.05$, 0.1, 0.15, 0.2 all fall exactly on a straight line. Another calculation has been performed for $\text{Re} = 200$, which renders $D = 43.9$, 34.3, and 30.5 corresponding to $t = 0.05$, 0.1, and 0.15, respectively. These

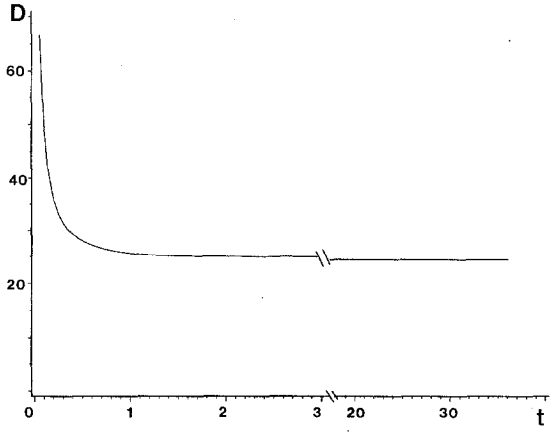

FIG. 2. Drag force D vs t at $\text{Re} = 400$ for the implusively starting flow.

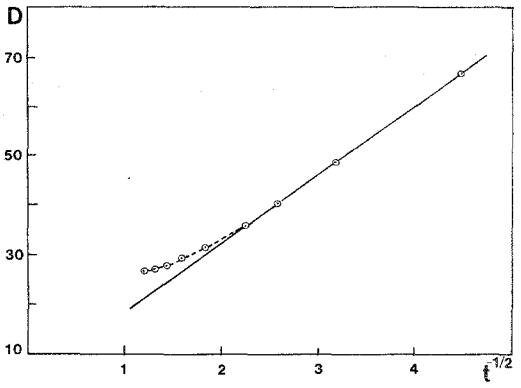

FIG. 3. Drag force D vs $t^{-1/2}$ using $\Delta t = 0.05$.

values of D are also on a straight line if plotted against $t^{-1/2}$. Therefore, we can say that the drag force on the lid has a $t^{-1/2}$ singularity as $t \to 0^+$, and from these data

$$C_D = 0.035\, t^{-1/2} \qquad \text{for} \quad t \to 0^+. \tag{25}$$

Since the coefficient in (25) is the same for both $\mathrm{Re} = 400$ and 200, it may well be considered as a universal constant at least for the Reynolds number range considered here. This type of singularity in the drag can be expected from the previous boundary layer considerations (i.e., $\delta \sim \sqrt{t/\mathrm{Re}}$ as $t \to 0^+$). If Δt is taken much smaller, 0.01, for instance, we can, of course, obtain a numerically stable solution. However, it must be determined if the solution obtained is physically acceptable for $t \to 0^+$. By (24), our estimate of the shear $\partial u/\partial y$ at $y = 1$ with $u_{\mathrm{lid}} = 1$, $u_{jJ} = u_{iJ-1} = 0$, and $\Delta y = 1/40$ is about 107. This is approximately the maximum

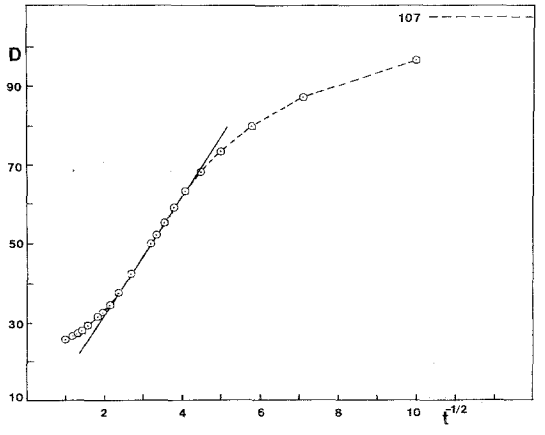

FIG. 4. Drag force D vs $t^{-1/2}$ using $\Delta t = 0.01$.

shear to be yielded from the grid size in the present calculations, and this maximum replaces the very high physical shear values $\partial u/\partial y$ that approach infinity as $t \to 0^+$. This is entirely a grid effect and is nonphysical. The values of D obtained using $\Delta t = 0.01$ are also plotted against $t^{-1/2}$ in Fig. 4, which shows that D approaches a fixed asymptotic value, presumably 107. Even though this asymptotic behavior for $t \to 0^+$ is not physical, in a very short time (e.g., $t \gtrsim 0.05$) D varies linearly with $t^{-1/2}$, and the slope calculated from this linear regime in Fig. 4 is the same as the coefficient given in (25). Therefore, it can be said that after the impulsive start there is a period of time in which the numerical solution depends solely upon the grid and is nonphysical if too small a value of time step Δt is used. On the other hand, if

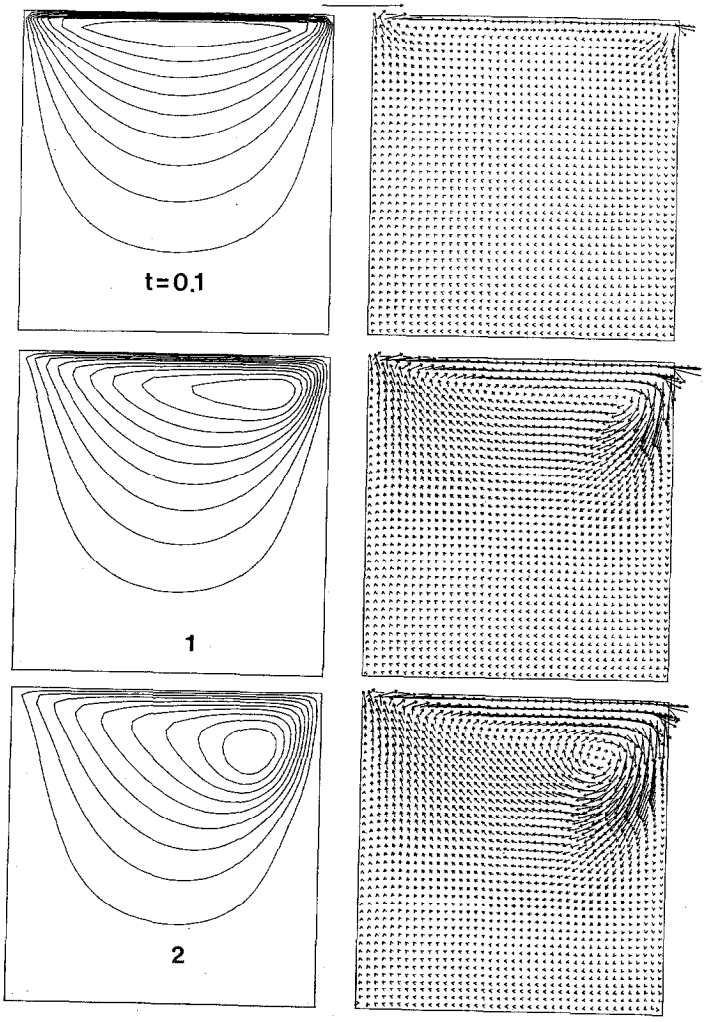

FIG. 5. Flow evolution for the implusively starting flow.

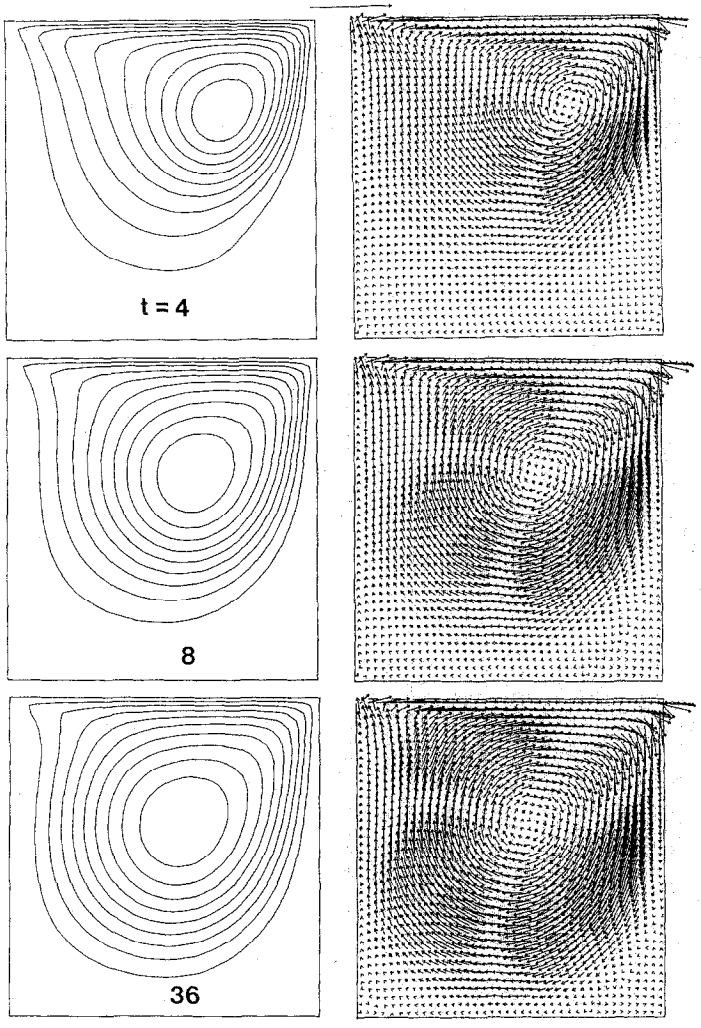

FIG. 5—*Continued.*

we take Δt large at the beginning, then the step function given as the initial condition at the lid may be misread as a uniform acceleration of $U_0/\Delta t$, so that a solution with different initial condition is obtained. For a physically interpretable solution during the early stages of the flow evolution, neither too small nor too large a time step should be used for a given grid. A solution that is to be physically interpreted for $t \ll 1$ may be obtained using a much finer or a stretched grid. Even for a small Δt with a finer grid, an implicit approach is recommended since reducing the grid size imposes severe limitations on the time step size if an explicit time advancing method is used.

Flow development with time is shown in Fig. 5 by presenting both streamline

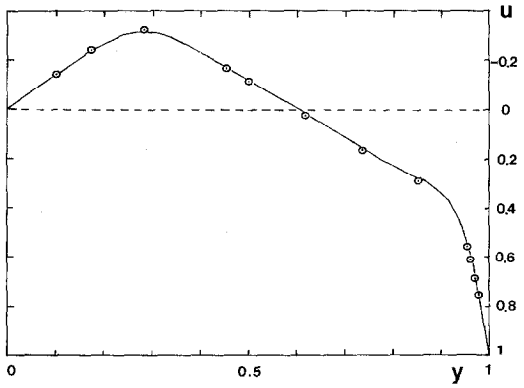

FIG. 6. u-velocity profile on the axis $x = 0.5$ for $\mathrm{Re} = 400$: ○, Ghia *et al.* [13]; –, present calculation.

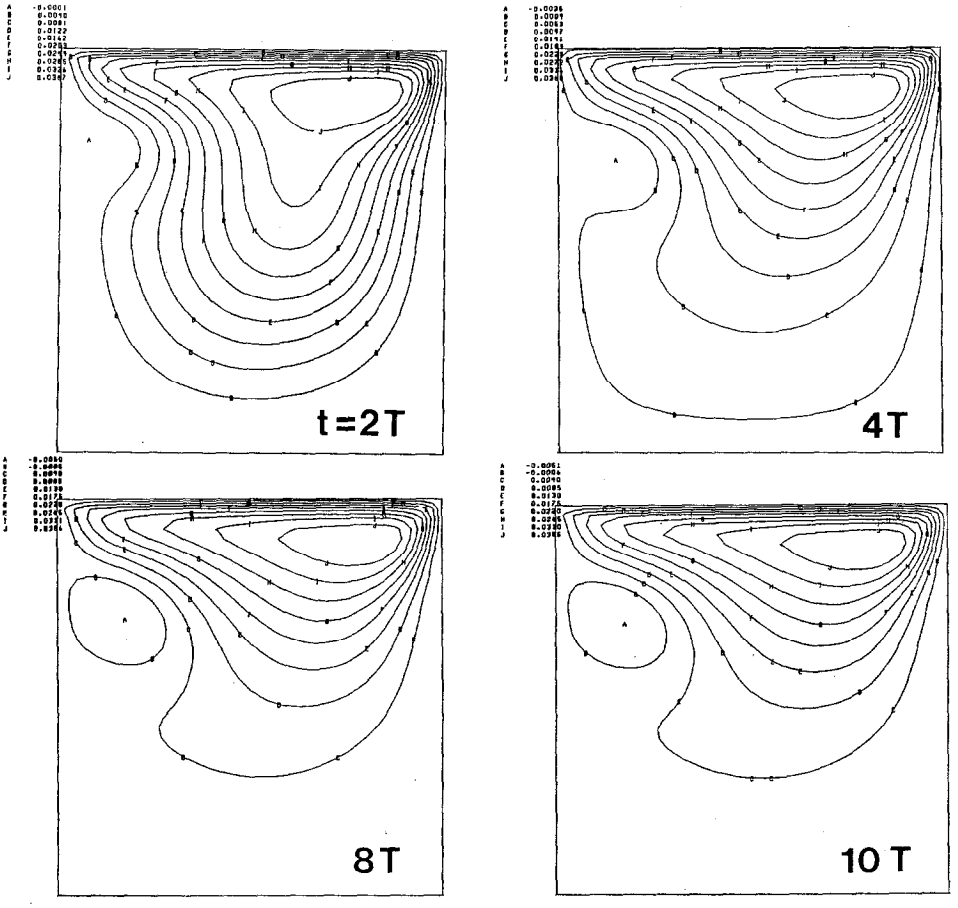

FIG. 7. History of the flow from steady state to the periodic state.

contours and velocity vector plots. At the beginning the streamline contours appear symmetric about the axis $x = 0.5$ as shown at $t = 0.1$. The boundary layer appears clearly just beneath the lid as crowded streamlines. Flow change is limited to the region very close to the lid and the fluid remains stagnant in the rest of the cavity. Immediately after the impulsive start of the lid, the flow exhibits a large vortical structure with a vortex center located at about $x = 0.5$ and very close to the lid. As the flow evolves the vortex center moves towards $x = 1$ as shown at $t = 1$ and 2. As the vortex approaches the right wall at $x = 1$, an interaction occurs between the vortex and the wall, and the vortex retreats from the wall while its center continuously drops. This is illustrated in Fig. 5 for $t = 1$, 2, and 4. Counter rotating vortices appear near the right and the left corners in the lower cavity as early as $t = 2$, and grow in size as the flow evolves further. This is shown in the vector plots at $t = 2$, 4, 8, in Fig. 5. The magnitude of velocity in these additional recirculating regions is extremely small.

The values of $\max(\partial u/\partial t)$ and $\max(\partial v/\partial t)$ are about 7.3 and 3.7 at $t = 0.05$ and become smaller with time. At $t = 36$ near the right corner in the upper cavity these values are about 8×10^{-4} and 1×10^{-3}, which are reasonably small for the assumption of the steady state, especially in areas away from the corners. The u-velocity profile at $x = 0.5$, which is the axis of geometric symmetry for the cavity, is compared at $t = 36$ with the steady solution of Ghia *et al.* [13] in Fig. 6.

Oscillatory Flow

As the second computational result we present a fluid flow in a driven cavity with a time-periodic lid velocity. The oscillating lid velocity is given as

$$U_B(t) = U_0 \cos \omega t,$$

where ω is the frequency, with period $T = 2\pi/\omega$. In this study we will take $\omega = 1$.

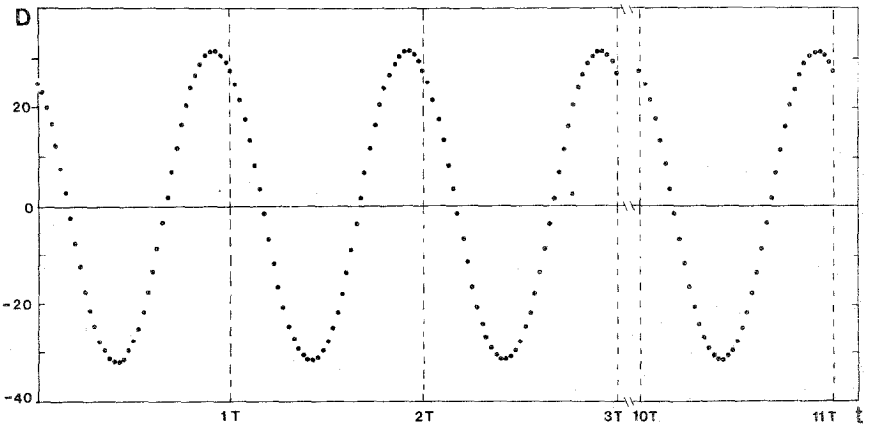

FIG. 8. Drag force D vs t.

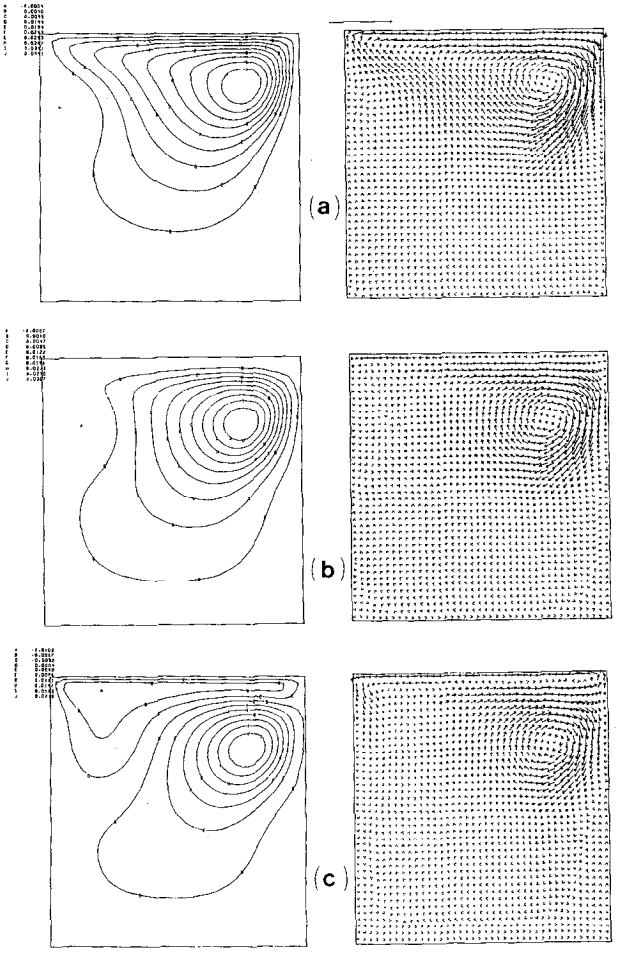

FIG. 9. Flow patterns inside one complete cycle after time periodicity is attained in the solution.

The Reynolds number is 400 based upon the maximum lid velocity U_0. The steady solution for the previous example is used as the initial data for the flow variables **u** and p at $t=0$. One period or cycle is divided into 40 uniform time intervals, so that $\Delta t = 2\pi/40$ for this calculation. This problem can be viewed as a driven cavity flow in which the lid is given succesive impulses with a step increase in lid velocity of $U_B(t+\Delta t) - U_B(t)$.

In this example we set β and $\Delta\tau$ at 50 and 20, respectively. The convergence criterion for the steady state in pseudo-time is taken as $\max(E_v) < 3\times 10^{-3}$. The number of pseudo-time steps required to reach the steady state are $50-80$. The values of $\max(\nabla\cdot\mathbf{u})$, $\max(E_u)$, $\mathrm{rms}(E_u)$, and $\mathrm{rms}(E_v)$ become $1.2\times 10^{-5}-5\times 10^{-6}$, $1.5\times 10^{-6}-3\times 10^{-7}$, $7\times 10^{-5}-3\times 10^{-5}$, $5.3\times 10^{-6}-1.8\times 10^{-6}$, and 2.7×10^{-4}

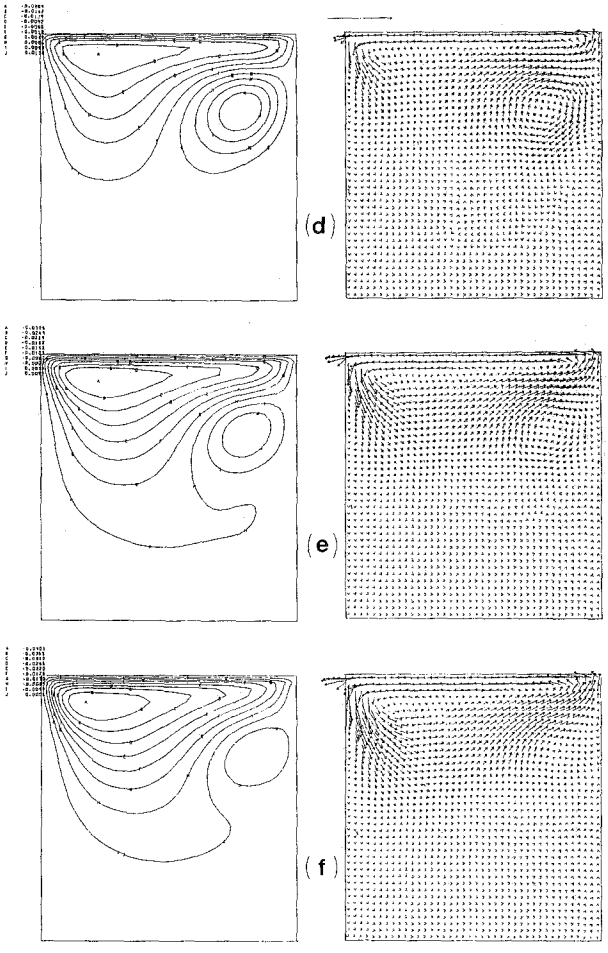

FIG. 9—*Continued.*

-1.4×10^{-4}, respectively. The Navier–Stokes equations must be integrated in time for as many cycles as are needed to reach a periodic steady state. In the periodic steady state the solutions at time t and $t + T$ must be identical. For the present case, about 8 cycles are required to reach the periodic steady state from initial data given by the previous solution at $t = 36$.

Figure 7 illustrates the evolution of the flow at times when U_B reaches its positive maximum at $t = mT$ for $m = 2$, 4, 8, and 10. The contour plot for $m = 0$ corresponds to the steady solution of the previous problem that was taken as the initial data for this computation. Since the streamline contours for $m = 8$ and $m = 10$ appear identical, we assume that the periodic steady state is obtained for $m \geq 8$. The drag force

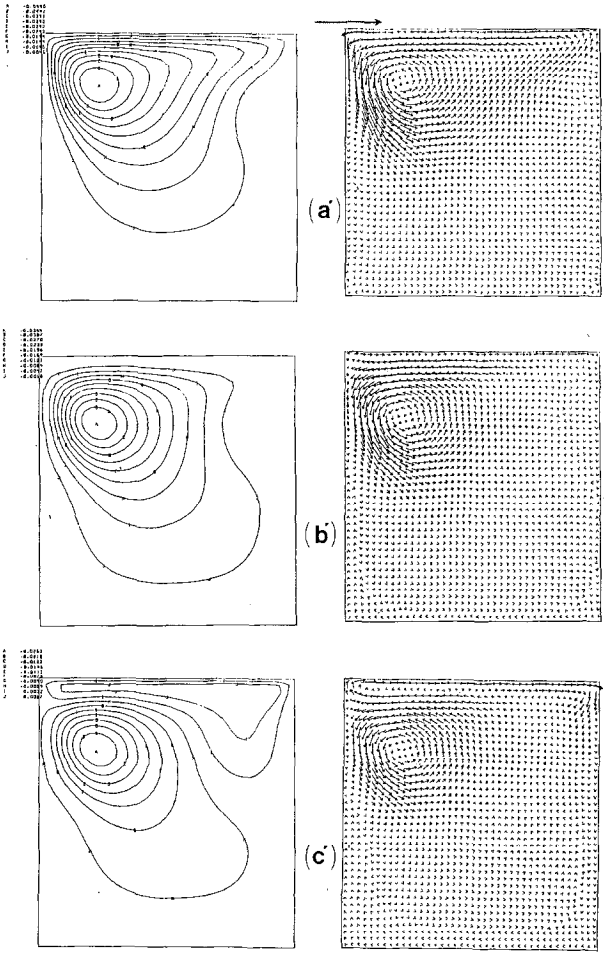

FIG. 9—*Continued.*

be seen by comparing the magnitude and the shift of the first valley with those that come afterward in Fig. 8. Like the previous example, it takes many more cycles to obtain the periodic steady solution for the entire flow field. The asymptotic maximum drag for this problem is about $D = 31.4$. Figure 8 shows that there is 31.5° phase shift with the maximum drag occuring about $3.5\Delta t$ before the lid reaches its peak velocity.

Streamline contours and velocity vector plots for the periodic steady solution are presented in Fig. 9 at the 11th cycle for $10T < t \leqslant 11T$. Figures 9a through f' correspond, in order, to the time sequence $t = 10T + \gamma\Delta t$, where $\gamma = 8$, 12, 14, 16, 18, 20, 28, 32, 34, 36, 38, and 40. A symmetry consideration leads us to expect that flows at time t and $t + T/2$ are mirror images of each other about $x = 0.5$, and the

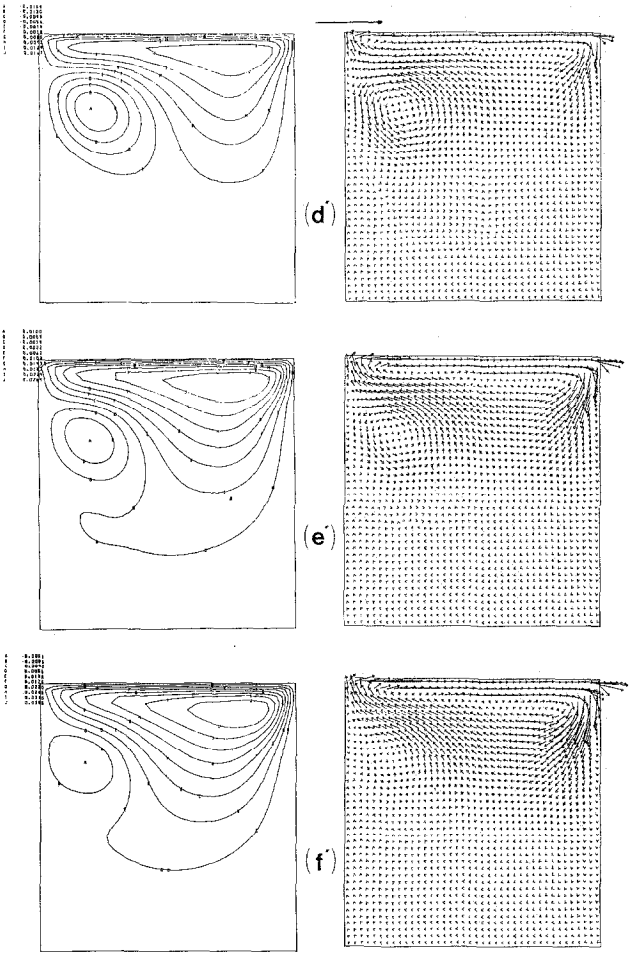

FIG. 9—*Continued.*

streamline contours and velocity vector plots clearly indicate the symmetry between Figs. 9a–f and a′–f′.

4. SUMARRY

A time and space accurate numerical method has been presented for the solution of the incompressible Navier–Stokes equations. The divergence-free velocity constraint and the nonlinearities have been dealt with at each physical time step by using a straightforward time-marching method in pseudo-time with artificial compressibility. With the present method we can extract the $t^{-1/2}$ singularity in the drag

on the lid for the impulsively started cavity flow and also obtain a crisp periodicity in the solution of the oscillatory motion.

REFERENCES

1. J. FROMM, The time dependent flow of an incompressible viscous fluid, *Methods Comput. Phys.* **3**, 345 (1964).
2. A. J. CHORIN, *Math. Comput.* **22**, 745 (1968).
3. J. KIM AND P. MOIN, *J. Comput. Phys.* **59**, 308 (1985).
4. C. W. HIRT AND J. L. COOK, *J. Comput. Phys.* **10**, 324 (1972).
5. R. PEYRET, *J. Fluid Mech.* **78**, 49 (1976).
6. F. H. HARLOW AND J. E. WELCH, *Phys. Fluids* **8**, 2182 (1965).
7. G. P. WILLIAMS, *J. Fluid Mech.* **37**, 727 (1969).
8. P. MOIN AND J. KIM, *J. Comput. Phys.* **35**, 381 (1980).
9. A. J. CHORIN, *J. Comput. Phys.* **2**, 12 (1967).
10. J. L. C. CHANG AND D. KWAK, *AIAA Paper* 84-0252 (1984).
11. W. Y. SOH, *J. Fluid Mech.* **188**, 337 (1988).
12. W. Y. SOH, *J. Comput. Phys.* **70**, 232 (1987).
13. U. GHIA, K. N. GHIA, AND C. T. SHIN, *J. Comput. Phys.* **48**, 387 (1982).
14. R. SCHREIBER AND H. B. KELLER, *J. Comput. Phys.* **48**, 310 (1982).
15. S. P. VANKA, *J. Comput. Phys.* **65**, 138 (1986).
16. T. B. GATSKI, C. E. GROSCH, AND M. E. ROSE, *J. Comput. Phys.* **48**, 1 (1982).
17. C. J. CHEN AND H. C. CHEN, *J. Comput. Phys.* **53**, 209 (1984).
18. K. GUSTAFSON AND K. HALASI, *J. Comput. Phys.* **64**, 279 (1986).
19. K. GUSTAFSON AND K. HALASI, *J. Comput. Phys.* **70**, 271 (1987).